12

Two-spin and parity-violating single-spin asymmetries at large scale

Besides inclusive deep inelastic lepton–hadron scattering, which was treated in detail in Chapter 11, there is an enormous amount of data on spin dependence in a wide variety of other reactions, inclusive, semi-inclusive and exclusive, and at a range of momentum transfers from zero (forward scattering) to moderately large values $p_T^2 \lesssim 8$ $(\mathrm{GeV}/c)^2$. Also there is the prospect of a huge increase in p_T with the coming into operation of the polarized RHIC collider at Brookhaven. Broadly speaking the large-momentum-transfer reactions or those involving some large scale can be treated using perturbative QCD; however, there is a major distinction between inclusive or semi-inclusive reactions, where the parton densities play a crucial rôle, and exclusive reactions where, in principle, one needs to know the parton *wave function* of the hadron. Our knowledge of the latter is much less secure than that of the parton densities.

As for the reactions at small momentum transfer, with no large mass scale, they fall into the regime of non-perturbative QCD and are presently treated in a less fundamental way. Indeed there is really no satisfactory theoretical explanation of the dramatic spin dependence seen in many of these reactions. This will be discussed in Chapter 14.

There is a further distinction between *single-spin asymmetries*, such as the polarization of a particle produced in an unpolarized collision or the analysing power of a reaction, and *double-spin asymmetries* such as the dependence of a cross-section upon the initial spins in the collision of a polarized beam on a polarized target. There are two types of single-spin asymmetry: helicity or longitudinal spin asymmetries, which are parity violating and occur in electroweak processes such as the production of massive lepton–antilepton pairs involving γ–Z^0 interference, or the production of $W^{\pm}$; and transverse spin asymmetries, which, as will be seen in Chapter 13, are difficult to generate in perturbative QCD.

https://doi.org/10.1017/9781009402040.012 Published online by Cambridge University Press

The double-spin asymmetries, however, will be seen to emerge in a very natural way from perturbative QCD. Indeed partonic reactions have very large double-spin asymmetries and the relation between hadronic and partonic asymmetries will play a crucial rôle in gaining further insight into the polarized-parton densities discussed in Chapter 11. This subject is about to take a major leap forward with the coming into operation of RHIC, where two beams of 250 GeV polarized protons will collide head on. For the first time ever it will be possible to study proton–proton spin asymmetries at truly high energies and truly large momentum transfers. At the same time COMPASS will begin to produce results on semi-inclusive deep inelastic lepton–hadron scattering, promising much new information about the polarized densities of antiquarks and gluons.

12.1 Inclusive and semi-inclusive reactions: general approach

In the following we concentrate largely on hadron–hadron collisions, but lepton–hadron reactions are mentioned in subsection 12.2.5.

Consider the hadronic collision

$$A + B \to C + X \tag{12.1.1}$$

in which C is produced with large transverse momentum p_T. The product C could be a jet, a specific hadron, a lepton–antilepton pair (the Drell–Yan reaction) or an electroweak gauge boson. In practice A and B will be protons or antiprotons.

For a hadronic final state the reaction is visualized as in Fig. 12.1 and is interpreted in a probabilistic sense. The beam and target are simply sources of partons, the parton number densities being either known from deep inelastic scattering or parametrized in some simple form. Partons from A and B undergo a large p_T collision, the *partonic subprocess*, which is calculated perturbatively, and one of the final state partons may then *hadronize* into C. The hadronization, being non-perturbative, is treated phenomenologically in terms of a *fragmentation* function.

In order to understand the spin structure, consider a collision of longitudinally polarized protons that produces a particle C with large p_T. Ignore all momenta and all integrations and pretend that a quark of only one flavour from each proton participates in the reaction. Symbolically, then, Fig. 12.1 yields

$$d\sigma_{\Lambda\Sigma} \sim \sum_{\lambda,\sigma,\rho} q_\lambda^\Lambda q_\sigma^\Sigma d\hat{\sigma}_{\rho;\lambda\sigma} D_C^\rho \tag{12.1.2}$$

where Λ, Σ are the proton helicities, λ and σ the helicities of the quarks, $d\hat{\sigma}_{\rho;\lambda\sigma}$ the quark–quark differential cross-section for incoming quarks of

https://doi.org/10.1017/9781009402040.012 Published online by Cambridge University Press

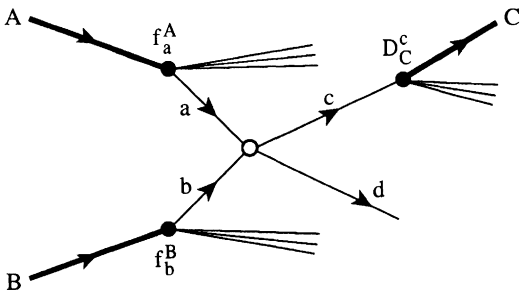

Fig. 12.1 Mechanism for $AB \to CX$ in the parton model. Heavy lines represents hadrons, and light lines represent partons.

helicities λ and σ to produce a quark of helicity ρ, and D_C^ρ is the probability for the quark of helicity ρ to fragment into a C. If the spin of C is not measured the latter cannot, in fact, depend on ρ so can be left out in the following discussion.

We then have symbolically

$$d\sigma_{++} \sim q_+^+ q_+^+ d\hat{\sigma}_{++} + q_-^+ q_+^+ d\hat{\sigma}_{-+} + q_-^+ q_-^+ d\hat{\sigma}_{--} + q_+^+ q_-^+ d\hat{\sigma}_{+-}. \tag{12.1.3}$$

By parity invariance

$$d\hat{\sigma}_{++} = d\hat{\sigma}_{--} \qquad \text{and} \qquad d\hat{\sigma}_{+-} = d\hat{\sigma}_{-+} \tag{12.1.4}$$

so that (12.1.3) becomes

$$d\sigma_{++} \sim (q_+^+ q_+^+ + q_-^+ q_-^+) d\hat{\sigma}_{++} + (q_-^+ q_+^+ + q_+^+ q_-^+) d\hat{\sigma}_{+-}. \tag{12.1.5}$$

Similarly

$$d\sigma_{+-} \sim (q_+^+ q_+^- + q_-^+ q_-^-) d\hat{\sigma}_{++} + (q_-^+ q_+^- + q_+^+ q_-^-) d\hat{\sigma}_{+-} \tag{12.1.6}$$

but again, by parity invariance,

$$q_-^- = q_+^+ \qquad \text{and} \qquad q_+^- = q_-^+ \tag{12.1.7}$$

so that (12.1.6) becomes

$$d\sigma_{+-} \sim (q_+^+ q_-^+ + q_-^+ q_+^+) d\hat{\sigma}_{++} + (q_-^+ q_-^+ + q_+^+ q_+^+) d\hat{\sigma}_{+-}. \tag{12.1.8}$$

Finally then

$$\begin{aligned} d\sigma_{++} - d\sigma_{+-} &\sim (q_+^+ \Delta q - q_-^+ \Delta q) d\hat{\sigma}_{++} + (q_-^+ \Delta q - q_+^+ \Delta q) d\hat{\sigma}_{+-} \\ &= \Delta q \Delta q d\hat{\sigma}_{++} - \Delta q \Delta q d\hat{\sigma}_{+-} \\ &= \Delta q \Delta q d\Delta\hat{\sigma} \end{aligned} \tag{12.1.9}$$

where, as in Section 11.3, $\Delta q = q_+^+ - q_-^+$ and $d\Delta\hat{\sigma} = d\hat{\sigma}_{++} - d\hat{\sigma}_{+-}$.

The spin structure in (12.1.9) is quite general and will always emerge if Fig. 12.1 is interpreted probabilistically.

https://doi.org/10.1017/9781009402040.012 Published online by Cambridge University Press

In detail, let $f_a^A(x_a)$ be the number density of partons of type a in hadron A and let $D_C^c(z)$ be the fragmentation function for parton c to fragment into C, with C having a fraction z of the parton's momentum.

Then for the unpolarized differential cross-section for $AB \to CX$, where C has energy E_C and momentum $\mathbf{p}_C = (\mathbf{p}_T, p_z)$,

$$E_C \frac{d^3\sigma}{d^3\mathbf{p}_C} = \frac{1}{\pi} \sum_{a,b,c,d} \int_{\xi_a} dx_a \int_{\xi_b} dx_b f_a^A(x_a) f_b^B(x_b) \times \left[\frac{d\hat{\sigma}^{ab\to cd}}{d\hat{t}}(\hat{s}, \hat{t}) \frac{1}{z} D_C^c(z) \right] \tag{12.1.10}$$

where the right-hand side is independent of the azimuthal angle ϕ and where $\hat{s}$, $\hat{t}$ are the Mandelstam variables for the partonic reaction

$$\hat{s} \equiv (p_a + p_b)^2 \simeq 2p_a \cdot p_b \simeq x_a x_b s \tag{12.1.11}$$

$$\hat{t} \equiv (p_a - p_c)^2 \simeq -2p_a \cdot p_c \simeq x_a t/z. \tag{12.1.12}$$

Here, for large momentum transfer,

$$s \equiv (p_A + p_B)^2 \simeq 2p_A \cdot p_B \tag{12.1.13}$$

$$t \equiv (p_A - p_C)^2 \simeq -2p_A \cdot p_C. \tag{12.1.14}$$

In (12.1.10) the value of z is fixed in terms of x_a and x_b, as follows. Let

$$x_T = \frac{2p_T}{\sqrt{s}} \tag{12.1.15}$$

be the ratio of p_T to its maximum allowed value, and define the rapidity by

$$y \equiv -\ln \tan \theta/2 \tag{12.1.16}$$

where θ is the production angle of C in the AB centre of mass frame. Then

$$z = \frac{x_T}{2} \left(\frac{e^y}{x_a} + \frac{e^{-y}}{x_b} \right). \tag{12.1.17}$$

In terms of these variables one has

$$\hat{t} = -\frac{s}{2} \left(\frac{x_a x_T}{z} \right) e^{-y} \tag{12.1.18}$$

$$\hat{u} \equiv (p_b - p_c)^2 = -\frac{s}{2} \left(\frac{x_b x_T}{z} \right) e^{y}. \tag{12.1.19}$$

The lower limits of integration in (12.1.10) are given by

$$\xi_a = \frac{x_T e^y}{2 - x_T e^{-y}} \qquad \xi_b = \frac{x_a x_T e^{-y}}{2x_a - x_T e^y}. \tag{12.1.20}$$

https://doi.org/10.1017/9781009402040.012 Published online by Cambridge University Press

The cross-section to produce a jet of energy E, momentum $\mathbf{p} = (\mathbf{p}_T, p_z)$ is obtained from (12.1.10) by summing over C, and making the replacement

$$\sum_C D_C^c(z) \to \delta(1-z) \tag{12.1.21}$$

and then carrying out the integration over x_b, which forces the equality

$$x_b = \frac{x_a x_T e^{-y}}{2x_a - x_T e^{y}}. \tag{12.1.22}$$

For the production of a hard photon,

$$A + B \to \gamma + X,$$

to order $\alpha\alpha_s$ the square bracket in (12.1.10) is replaced by

$$\frac{d\hat{\sigma}^{ab\to\gamma d}}{d\hat{t}}\,\delta(1-z) \tag{12.1.23}$$

and the relevant partonic subprocesses are $Gq \to \gamma q$ and $q\bar{q} \to \gamma G$. QCD corrections to order $\alpha\alpha_s^2$ involve also final states with three partons, e.g. $GG \to \gamma q\bar{q}$, with integration over the phase space of the additional parton.

As written eqn (12.1.10) is at the level of the simple parton model. Allowing for QCD corrections in the leading logarithmic approximation (the LLA, see Section 11.6) one simply makes the replacements

$$\begin{aligned} f_a^A(x_a) &\to f_a^A(x_a, Q^2) \\ D_C^c(z) &\to D_C^c(z, Q^2) \end{aligned} \tag{12.1.24}$$

where $Q^2 \approx p_T^2$ and the parton densities remain universal, i.e. the same densities appear in DIS and in all large-p_T reactions. When one goes beyond the LLA care must be taken with scheme dependence, and the densities that appear in one reaction will differ by terms of order $\alpha_s(Q^2)$ from the densities occurring in other reactions.

12.2 Longitudinal two-spin asymmetries

For longitudinally polarized beam and target and for a parity-conserving theory one conventionally defines

$$A_{\mathrm{LL}} = \frac{d\sigma_{++} - d\sigma_{+-}}{d\sigma_{++} + d\sigma_{+-}} \equiv \frac{d\Delta\sigma}{2d\sigma} \tag{12.2.1}$$

where $+$ and $-$ refer to the *helicities* and where $d\sigma$ is the unpolarized differential cross-section. According to the discussion leading to (12.1.9),

https://doi.org/10.1017/9781009402040.012 Published online by Cambridge University Press

and suppressing the Q^2-dependence (12.1.24),

$$E_C \frac{d^3\sigma}{d^3\mathbf{p}_C} = \frac{1}{\pi} \sum_{a,b,c,d} \int_{\xi_a} dx_a \int_{\xi_b} dx_b \, \Delta f_a^A(x_a) \Delta f_b^B(x_b) \times \left[\frac{d\Delta\hat{\sigma}^{ab\to cd}}{d\hat{t}}(\hat{s},\hat{t}) \frac{1}{z} D_C^c(z) \right] \tag{12.2.2}$$

where

$$\frac{d\Delta\hat{\sigma}}{d\hat{t}} = \frac{d\hat{\sigma}_{++}}{d\hat{t}} - \frac{d\hat{\sigma}_{+-}}{d\hat{t}} \equiv 2\hat{a}_{LL} \frac{d\hat{\sigma}}{d\hat{t}}. \tag{12.2.3}$$

Note that there is no dependence on the azimuthal angle ϕ in the above. The polarized-parton distributions are the helicity-dependent Δq, ΔG that appear in the spin-dependent structure function g_1 in polarized DIS (Sections 11.3 and 11.7). With the exception of the gluon, they are reasonably well determined; see Fig. 11.15.

The observable A_{LL} is particularly important because at the parton level the asymmetries

$$\hat{a}_{LL} = \frac{d\hat{\sigma}_{++} - d\hat{\sigma}_{+-}}{d\hat{\sigma}_{++} + d\hat{\sigma}_{+-}} \tag{12.2.4}$$

are very large on account of the helicity structure discussed in Section 10.4. The lowest-order expressions for the unpolarized cross-sections, and the expressions for $\hat{a}_{LL}$, due to Babcock, Monsay and Sivers (1979) and to Ranft and Ranft (1978), are listed in Tables 12.1 and 12.2 for all partonic processes, and shown in Fig. 12.2 as a function of the parton scattering angle θ^* in the parton–parton CM.

In Table 12.1, for purely strong interactions the cross-sections in the parton–parton CM are given by

$$\frac{d\hat{\sigma}}{d\hat{t}} = \frac{\pi\alpha_s^2}{\hat{s}^2} \overline{|M|^2}. \tag{12.2.5}$$

For cross-sections involving one photon in the initial or final state, we have

$$\frac{d\hat{\sigma}}{d\hat{t}} = \frac{\pi e_q^2 \alpha \alpha_s}{\hat{s}^2} \overline{|M|^2}, \tag{12.2.6}$$

where e_q is the quark electric charge, and for the process $q\bar{q} \to \gamma \to l\bar{l}$ we have

$$\frac{d\hat{\sigma}}{d\hat{t}} = \frac{\pi e_q^2 \alpha^2}{\hat{s}^2} \overline{|M|^2}. \tag{12.2.7}$$

Of course these large asymmetries get diluted by the rather small

https://doi.org/10.1017/9781009402040.012 Published online by Cambridge University Press

Table 12.1. Partonic cross-sections (for the normalization see eqns (12.2.5)–(12.2.7)). Note that qq' means that the quarks q' and q differ in flavour

Reaction	$\overline{\lvert M\rvert^2}$
$qq \to qq$	$\frac{4}{9}\left(\frac{\hat{s}^2+\hat{u}^2}{\hat{t}^2}+\frac{\hat{s}^2+\hat{t}^2}{\hat{u}^2}-\frac{2}{3}\frac{\hat{s}^2}{\hat{u}\hat{t}}\right)$
$q\bar{q} \to q\bar{q}$	$\frac{4}{9}\left(\frac{\hat{s}^2+\hat{u}^2}{\hat{t}^2}+\frac{\hat{u}^2+\hat{t}^2}{\hat{s}^2}-\frac{2}{3}\frac{\hat{u}^2}{\hat{s}\hat{t}}\right)$
$qq' \to qq'$ $q\bar{q}' \to q\bar{q}'$	$\frac{4}{9}\frac{\hat{s}^2+\hat{u}^2}{\hat{t}^2}$
$q\bar{q} \to q'\bar{q}'$	$\frac{4}{9}\frac{\hat{u}^2+\hat{t}^2}{\hat{s}^2}$
$q\bar{q} \to GG$	$\frac{8}{3}\left(\frac{4}{9}\frac{\hat{u}^2+\hat{t}^2}{\hat{u}\hat{t}}-\frac{\hat{u}^2+\hat{t}^2}{\hat{s}^2}\right)$
$GG \to q\bar{q}$	$\frac{9}{64}\left[\frac{8}{3}\left(\frac{4}{9}\frac{\hat{u}^2+\hat{t}^2}{\hat{u}\hat{t}}-\frac{\hat{u}^2+\hat{t}^2}{\hat{s}^2}\right)\right]$
$qG \to qG$ $\bar{q}G \to \bar{q}G$	$(\hat{u}^2+\hat{s}^2)\left(\frac{1}{\hat{t}^2}-\frac{4}{9}\frac{1}{\hat{u}\hat{s}}\right)$
$GG \to GG$	$\frac{9}{2}\left(3-\frac{\hat{u}\hat{t}}{\hat{s}^2}-\frac{\hat{u}\hat{s}}{\hat{t}^2}-\frac{\hat{s}\hat{t}}{\hat{u}^2}\right)$
$qG \to q\gamma$ $\bar{q}G \to \bar{q}\gamma$	$-\frac{1}{3}\left(\frac{\hat{u}}{\hat{s}}+\frac{\hat{s}}{\hat{u}}\right)$
$q\bar{q} \to \gamma G$	$\frac{8}{9}\left(\frac{\hat{u}}{\hat{t}}+\frac{\hat{t}}{\hat{u}}\right)$
$q\bar{q} \to \gamma \to l\bar{l}$	$\frac{4}{3}\frac{\hat{u}^2+\hat{t}^2}{\hat{s}^2}$

polarizations of the partons inside the hadron, so that $|A_{LL}| \ll |\hat{a}_{LL}|$. Nonetheless, measurable asymmetries survive and will be very useful in learning about the polarized gluon density, which, as mentioned, is poorly known from polarized DIS, and in improving the precision of the polarized sea-quark densities. We shall give a few illustrations involving reactions that will be studied by the COMPASS and HERMES groups and at the RHIC collider. We draw the reader's attention to the fact that these

https://doi.org/10.1017/9781009402040.012 Published online by Cambridge University Press

Table 12.2. Partonic longitudinal double-spin asymmetries

Reaction	$\hat{a}_{LL}$
$qq \to qq$	$\dfrac{\hat{u}^2(\hat{s}^2-\hat{u}^2)+\hat{t}^2(\hat{s}^2-\hat{t}^2)-\frac{2}{3}\hat{s}^2\hat{t}\hat{u}}{\hat{u}^2(\hat{s}^2+\hat{u}^2)+\hat{t}^2(\hat{s}^2+\hat{t}^2)-\frac{2}{3}\hat{s}^2\hat{t}\hat{u}}$
$q\bar{q} \to q\bar{q}$	$\dfrac{\hat{s}^2(\hat{s}^2-\hat{u}^2)-\hat{t}^2(\hat{u}^2+\hat{t}^2)+\frac{2}{3}\hat{u}^2\hat{s}\hat{t}}{\hat{s}^2(\hat{s}^2+\hat{u}^2)+\hat{t}^2(\hat{u}^2+\hat{t}^2)-\frac{2}{3}\hat{u}^2\hat{s}\hat{t}}$
$qq' \to qq'$ $q\bar{q}' \to q\bar{q}'$	$\dfrac{\hat{s}^2-\hat{u}^2}{\hat{s}^2+\hat{u}^2}$
$q\bar{q} \to q'\bar{q}'$	-1
$q\bar{q} \to GG$	-1
$GG \to q\bar{q}$	-1
$qG \to qG$ $\bar{q}G \to \bar{q}G$	$\dfrac{\hat{s}^2-\hat{u}^2}{\hat{s}^2+\hat{u}^2}$
$GG \to GG$	$\dfrac{-3+2\hat{s}^2/(\hat{u}\hat{t})+(\hat{u}\hat{t})/\hat{s}^2}{3-(\hat{s}\hat{u})/\hat{t}^2-(\hat{s}\hat{t})/\hat{u}^2-(\hat{u}\hat{t})/\hat{s}^2}$
$qG \to q\gamma$ $\bar{q}G \to \bar{q}\gamma$	$\dfrac{\hat{s}^2-\hat{u}^2}{\hat{s}^2+\hat{u}^2}$
$q\bar{q} \to \gamma G$	-1
$q\bar{q} \to \gamma \to l\bar{l}$	-1

and other spin asymmetries can also be used in testing for non-standard physical effects – supersymmetry, technicolour etc. – which we do not have space to discuss. A comprehensive discussion can be found in the review article by Bourrely, Renard, Soffer and Taxil (1989).

12.2.1 $pp \to \pi^0 X$

In the lower part of Fig. 12.3 we show $A_{LL}^{\pi^0}$ at $y = 0$ for the reaction $pp \to \pi^0 X$ as measured by the E581/704 collaboration at Fermilab (Adams *et al.*, 1991) at $p_{\mathrm{L}} = 200$ GeV/c, corresponding to $\sqrt{s} = 20$ GeV.

Before discussing the theoretical curves, two points should be noted.

(1) The range of p_T is small, $1 \leq p_T \leq 3.5$ GeV/c, and it is known that the *unpolarized* cross-section is poorly described by QCD in this region unless the partons are given some intrinsic transverse momentum of order $\langle k_T \rangle \approx 0.45$ GeV/c. Equation (12.2.2) can be generalized to

https://doi.org/10.1017/9781009402040.012 Published online by Cambridge University Press

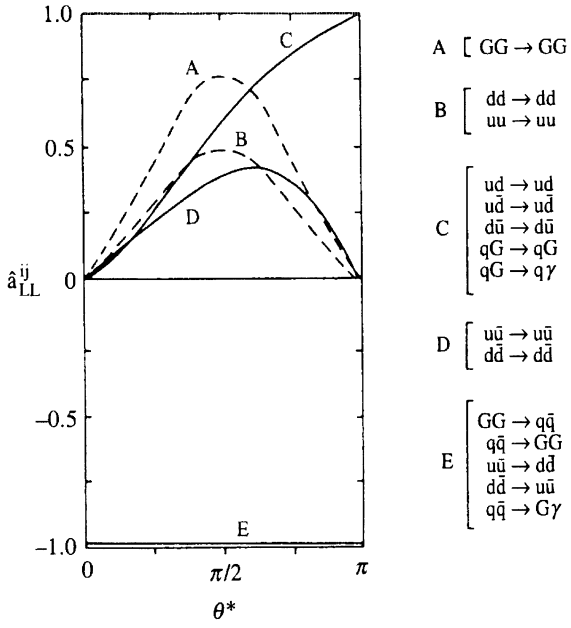

Fig. 12.2 Two-spin longitudinal asymmetry $\hat{a}_{LL}$ for various partonic reactions vs. CM scattering angle θ^*. (From Craigie, Hidaka, Jacob and Renard, 1983.)

allow for intrinsic k_T effects (Vogelsang and Weber, 1992), but this is a somewhat *ad hoc* procedure. Measurements at larger p_T will not be sensitive to k_T.

(2) The very small experimental asymmetries were claimed to prove that the polarized gluon density $\Delta G(x)$ is negligibly small, in contradiction with the use of ΔG to explain the 'spin crisis' discussed in Section 11.5. However, at the relatively small CM energy of 20 GeV, the p_T values involved imply, via (12.1.20), that typical x-values are outside the region where $\Delta G(x)$ is expected to be large (see Fig. 11.15).

The curves in the upper part of Fig. 12.3 correspond to a variety of $\Delta G(x)$, including a very hard version, (b), and a negative version, (c(−)); $-\Delta G(x)$ is shown for the case (c(−)). It is seen that the data have a very poor ability to discriminate amongst these, with the exception of (b), which is clearly ruled out. (A recent analysis of polarized DIS (Leader, Sidorov and Stamenov, 1998a) would rule out (b) as well as (c(±)); see Fig. 11.15.)

The general insensitivity to $\Delta G(x)$ in Fig. 12.3 is due to the low energy of the reaction and the fact that for the present data it is the $qG \to qG$

https://doi.org/10.1017/9781009402040.012 Published online by Cambridge University Press

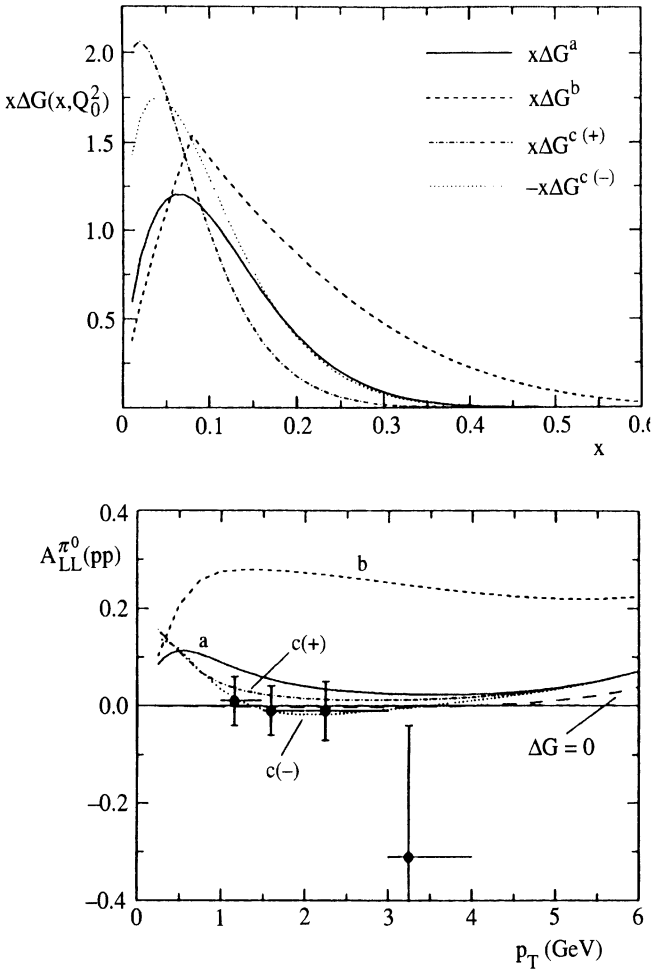

Fig. 12.3 Measured A_{LL} for $pp \to \pi^\circ X$ vs. p_T at $\sqrt{s} = 20$ GeV and $y = 0$ (Adams *et al.*, 1991) compared with theoretical predictions (Vogelsang, 1993) using various models of $\Delta G(x)$. The curves in the lower part of the figure correspond to the $\Delta G(x, Q^2)$ shown in the upper part at $Q^2 = 4(\text{GeV}/c)^2$. See the text for further explanation. (a) Kunszt (1989), (b) Ramsey and Sivers (1991) and (c) Glück, Reya and Vogelsang (1992).

process that dominates. At higher energies the reaction will be more discriminating.

12.2.2 Prompt photon production

It is expected that prompt photon production, $pp \to \gamma X$, will be rather sensitive to $\Delta G(x)$. The partonic process $qG \to q\gamma$ has a significant positive

https://doi.org/10.1017/9781009402040.012 Published online by Cambridge University Press

$\hat{a}_{LL}$ (see Fig. 12.2), while the competing process $q\bar{q} \to G\gamma$, although it has $\hat{a}_{LL} = -1$, is relatively unimportant because of the smallness of the polarized-sea density (see Fig. 11.15). A very detailed study, at next-to-leading order, has been carried out by Gordon and Vogelsang (1993, 1994).

Figure 12.4 shows $A_\gamma \equiv A_{LL}^\gamma$ versus p_T at $\sqrt{s} = 100$ GeV and $y = 0$ for two models of ΔG. Model (a) corresponds closely to the curve (a) in Fig. 12.3. It has a relatively large ΔG and the polarized sea-quark density is taken to be zero below a scale of $Q^2 = 10\ (\mathrm{GeV}/c)^2$. In model (b) the polarized gluon density is zero below $10\ (\mathrm{GeV}/c)^2$ and the polarized sea is relatively large and negative. It is seen that A_γ is quite sensitive to ΔG both in leading order and in next-to-leading order.

12.2.3 The Drell–Yan reaction $pp \to l^+l^-X$

The reaction, in lowest order, is visualized as in Fig. 12.5, where the lepton–antilepton pair is produced via virtual one-photon exchange $q\bar{q} \to$ 'γ' $\to l^+l^-$ and should thus be sensitive to the polarized antiquark density. For l^+l^- pairs of very large mass M it is also necessary to include Z^0 exchange and one then finds interesting single-spin parity-violating asymmetries as well (see subsection 12.3.3).

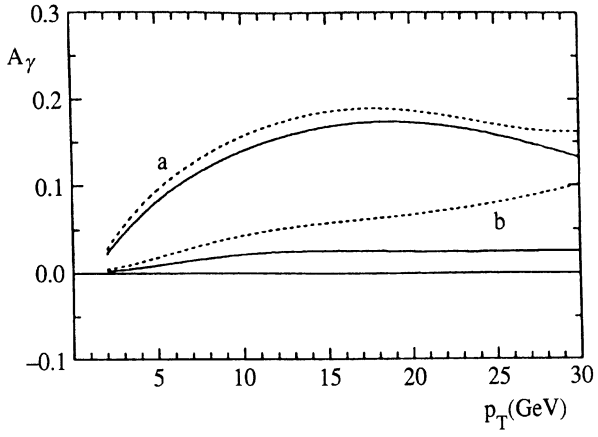

Fig. 12.4 Calculated values of $A_\gamma \equiv A_{LL}^\gamma$ for $pp \to \gamma X$ at $\sqrt{s} = 100$ GeV and $y = 0$ vs. p_T (from Vogelsang, 1993). The solid curves refer to next-to-leading order calculations and the broken curves to leading-order calculations for two models for ΔG (see text).

https://doi.org/10.1017/9781009402040.012 Published online by Cambridge University Press

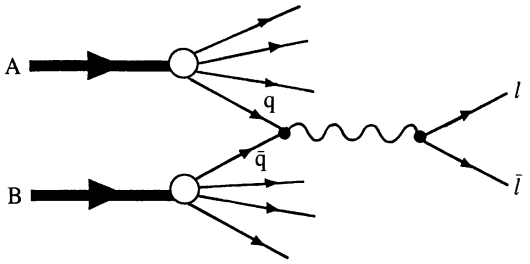

Fig. 12.5. Mechanism for the Drell–Yan reaction $pp \to l^+l^-X$ in lowest order.

Conventionally we define

$$\tau = \frac{M^2}{s} \tag{12.2.8}$$

and 'Feynman x'

$$x_{\mathrm{F}} = \frac{2}{\sqrt{s}} p_z \tag{12.2.9}$$

where p_z is the longitudinal momentum of the *pair*, which, in the lowest-order process, moves essentially along the pp collision axis. We then find that x_a and x_b are fixed once τ and x_{F} are determined:

$$x_a x_b = \tau \tag{12.2.10}$$

$$x_a - x_b = x_{\mathrm{F}}. \tag{12.2.11}$$

Since $x_{a,b}$ are fixed the result (12.2.2) simplifies greatly and one ends up with

$$A_{LL}^{\mathrm{D-Y}} = -\frac{\sum_f e_f^2 \left[\Delta q_f(x_a)\Delta\bar{q}_f(x_b) + \Delta q_f(x_b)\Delta\bar{q}_f(x_a)\right]}{\sum_f e_f^2 \left[q_f(x_a)\bar{q}_f(x_b) + q_f(x_b)\bar{q}_f(x_a)\right]} \tag{12.2.12}$$

where the sum is over the flavours f and where the parton densities should be evaluated at a scale $Q^2 \approx M^2$.

Equation (12.2.12) can be given a simple intuitive interpretation. Since the protons are just 'beams' of partons, (12.2.12) expresses the fact that

$$A_{LL}^{\mathrm{D-Y}} = \langle P_q P_{\bar{q}} \rangle_{x_a, x_b} \hat{a}_{LL}^{q\bar{q}\to l^+l^-} \tag{12.2.13}$$

where $\langle P_q P_{\bar{q}} \rangle$ plays the rôle of the product of quark and antiquark degrees of polarization and where, for the Drell–Yan process, $q\bar{q} \to \gamma \to l^+l^-$, $\hat{a}_{LL} = -1$.

A remarkable simplification can be achieved by a careful choice of the kinematics. Consider only events with $x_{\mathrm{F}} \gtrsim 0.2$. Then $x_a \gtrsim 0.2 + x_b$ and by keeping τ not too small, via (12.2.10) one can avoid very small x_b-values.

https://doi.org/10.1017/9781009402040.012 Published online by Cambridge University Press

For such a range of x_a, only the up quark is important in the denominator of (12.2.12). Moreover $\Delta s(x_a)$ is then negligible, so that

$$A_{LL}^{\mathrm{D-Y}} \simeq -\frac{1}{u(x_a)\bar{u}(x_b)}\left[\Delta u(x_a)\Delta\bar{u}(x_b) + \tfrac{1}{4}\Delta d(x_a)\Delta\bar{d}(x_b)\right]. \qquad (12.2.14)$$

Further, *in this region*, one can take for DIS (see (11.4.5))

$$\begin{aligned} F_1^p(x) &\approx \frac{2}{9}u(x) \\ g_1^p(x) &\approx \frac{1}{18}\left[4\Delta u(x) + \Delta d(x)\right] \\ g_1^n(x) &\approx \frac{1}{18}\left[\Delta u(x) + 4\Delta d(x)\right]. \end{aligned} \qquad (12.2.15)$$

Now $g_1^n(x)$ is almost zero for the region $0.25 \leq x \leq 0.5$ (see Figs. 11.13 and 11.14), suggesting that $\Delta d(x) \approx -\Delta u(x)/4$. Using this, (12.2.13) takes the beautifully simple form

$$A_{LL}^{\mathrm{D-Y}}(x_a, x_b) = -A_1(x_a)\frac{\Delta\bar{u}(x_b)}{\bar{u}(x_b)} \qquad x_a \gtrsim 0.2 + x_b \qquad (12.2.16)$$

where $A_1(x)$ is one of the two photon–proton asymmetries often used in discussing polarized DIS,

$$A_1(x) = \frac{g_1^p(x)}{F_1^p(x)} \qquad (12.2.17)$$

and its value is therefore known from experiment. Equation (12.2.16) thus provides a tight link between D–Y asymmetries and $\Delta\bar{u}$. Note that although radiative corrections are known to have a significant effect upon the lowest-order result for the cross-section, Ratcliffe (1983) showed that the result (12.2.12) is a good approximation. For a more complete study of NLO corrections, see Gehrmann (1997).

It should soon become possible to study the Drell–Yan reaction for an l^+l^- pair, in which the pair has large mass M and may have large p_T. This would involve the additional partonic process

$$q\bar{q} \to (\gamma \text{ or } Z^0) + G \qquad (12.2.18)$$

$$qG \to (\gamma \text{ or } Z^0) + q. \qquad (12.2.19)$$

The basic two-spin asymmetry $A_{LL}^{\mathrm{D-Y}}$ now becomes a function of x_T and the rapidity y of the pair, (see (12.1.15) and (12.1.16), and involves an integration over x_a, x_b subject to (12.1.22), so is not so directly related as before to the parton densities at specific x_a and x_b. However, as shown by Leader and Sridhar (1994), it does now becomes sensitive to the polarized gluon distribution. Moreover, there are other interesting asymmetries accessible if one can measure the distribution in the polar

angle θ_l of the lepton l^- in the l^+l^- rest frame, in which the axis OZ is chosen along the direction of the pair in the CM of the reaction.

The cross-section takes the form

$$\frac{d^4\sigma_{++/+-}}{dx_T dy d\tau d\cos\theta_l} = \sum_{j=0}^{2} D^j_{++/+-} Y_{j0}(\theta_l) \tag{12.2.20}$$

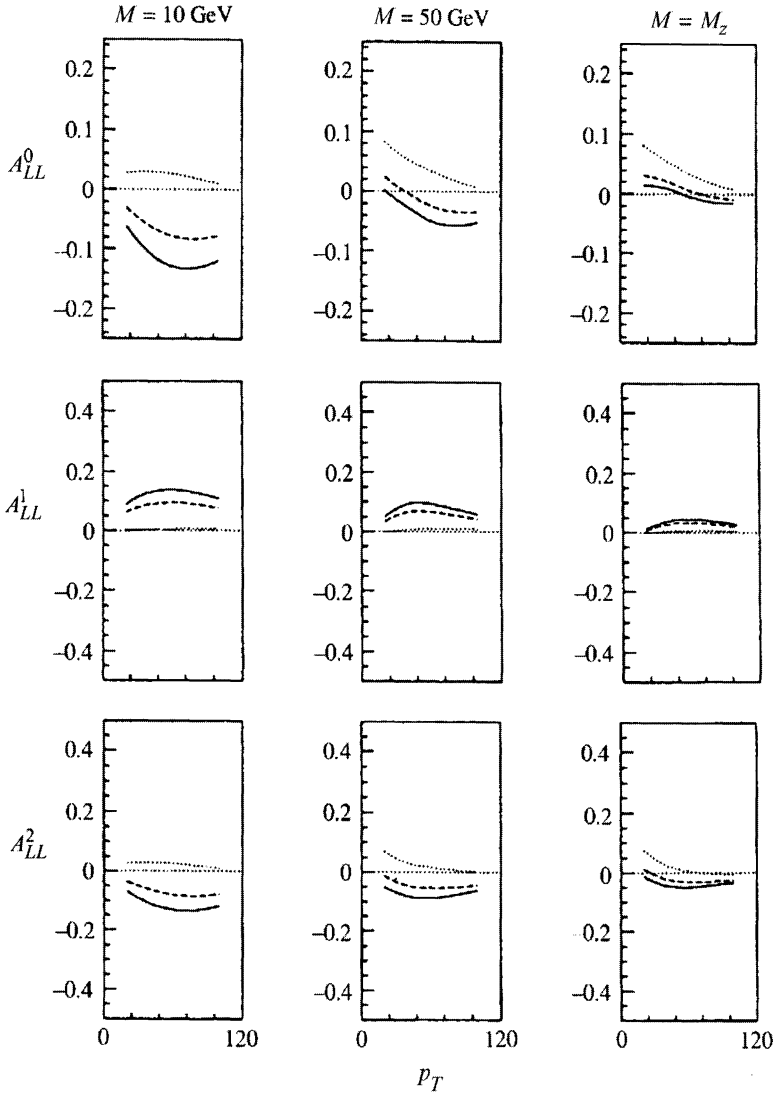

Fig. 12.6 The Drell–Yan asymmetries A^j_{LL} vs. p_T for several values of M and at $y = 0$. Solid curves; set I; broken curves, set II; dotted curves, set III. See the text for further explanation. (From Leader and Sridhar, 1994.)

https://doi.org/10.1017/9781009402040.012 Published online by Cambridge University Press

where the Y_{j0} are spherical harmonics and the coefficients D^j depend on x_T, y and τ and involve an integration over the momentum fractions carried by the partons. Explicit expressions can be found in Leader and Sridhar (1994).

There are then three double spin asymmetries[1] $j = 0, 1, 2$:

$$A_{LL}^{j} = \frac{D_{++}^{j} - D_{+-}^{j}}{D_{++}^{j} + D_{+-}^{j}} \tag{12.2.21}$$

of which $A_{LL}^{0} \equiv A_{LL}^{\mathrm{D-Y}}$.

Some results are shown in Fig. 12.6 as functions of p_T, for various pair masses, and for $y = 0$. The curves correspond to the three kinds of polarized gluon density given in Sridhar and Leader (1992).

set I (solid curves), ΔG large, $\Delta s = 0$;
set II (broken curves), ΔG and Δs both moderately large; (12.2.22)
set III (dotted curves), $\Delta G = 0$, Δs large.

It is seen that these double-spin asymmetries are reasonably large and offer some hope of discriminating between the various models of ΔG.

Another interesting possibility, suggested by Contogouris and Papadopoulos (1991), is to look for longitudinal spin correlations with only one of the initial hadrons longitudinally polarized and with detection of the longitudinal polarization of one of the produced leptons. Perhaps this is feasible for $\mu^+\mu^-$ production.

The above suggestions look somewhat futuristic, since so far there have been no experiments on polarized Drell–Yan reactions; they will be studied for the first time at the polarized pp collider RHIC, which came into operation early in the year 2000.

12.2.4 Drell–Yan production of J/Ψ and χ_2

We comment briefly upon the possibility of using these reactions to learn about ΔG. The most important partonic processes are shown in Fig. 12.7 and are gluon initiated. The processes shown in Fig. 12.8 are much less important.

Note that in process A in Fig. 12.7

$$x_a x_b = M_{\chi}^2 / s \tag{12.2.23}$$

[1] These are referred to as A_{d}^{j} (d for double) in the above-cited paper.

https://doi.org/10.1017/9781009402040.012 Published online by Cambridge University Press

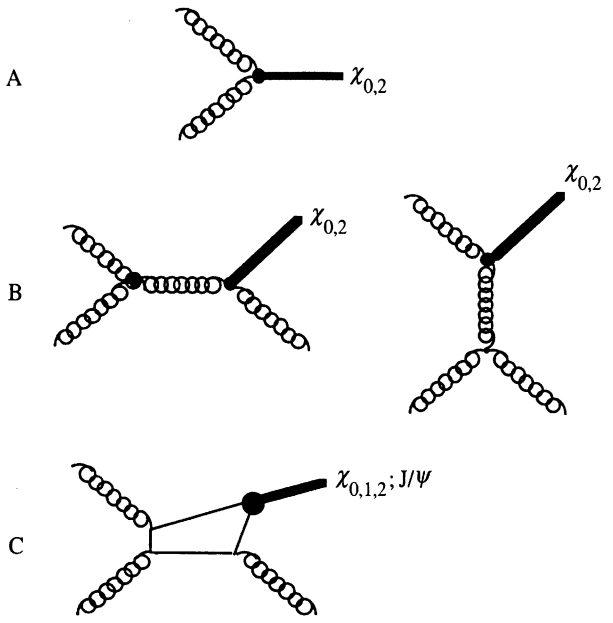

Fig. 12.7. The most important partonic reactions involved in $pp \to J/\Psi$ or $\chi_2 + X$.

whereas in processes B and C

$$1 \geq x_a x_b \geq M_{\tilde{\chi}}^2/s. \tag{12.2.24}$$

χ_2 *production.* This is very clean when reaction A of Fig. 12.7 dominates and, as pointed out by Cortes and Pire (1988), should have a large asymmetry since the partonic asymmetry is maximal,

$$\hat{a}_{LL}^{GG\to\chi_2} = -1. \tag{12.2.25}$$

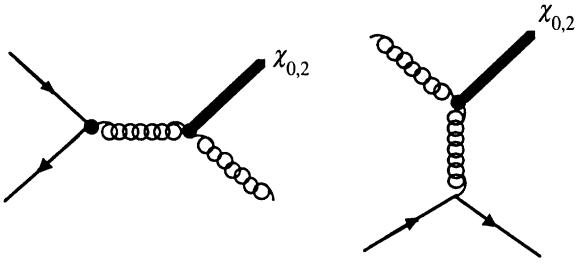

Fig. 12.8. Less important ($q\bar{q}$ initiated) partonic reactions.

https://doi.org/10.1017/9781009402040.012 Published online by Cambridge University Press

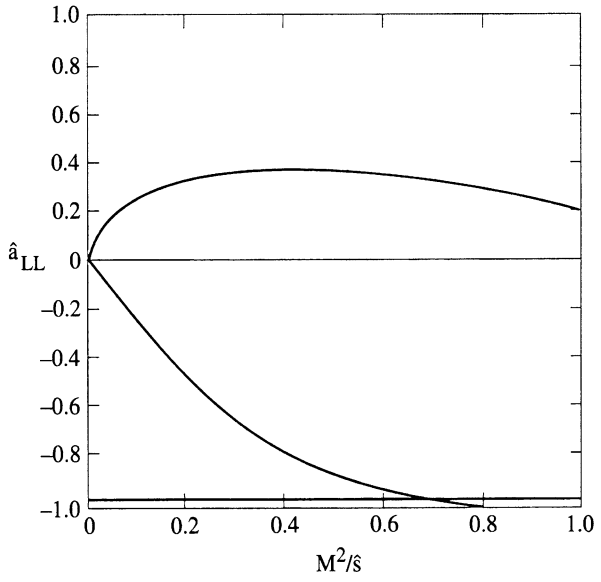

Fig. 12.9 Longitudinal partonic asymmetry for (top curve) $GG \to J/\Psi + G$, (bottom curve) $GG \to \chi_2$ and (middle curve) $GG \to \chi_2 + G$, extracted from the results of Doncheski and Robinett (1994). See the text for an explanation of the curves.

At low energies reaction A should dominate, in which case knowing x_F fixes x_a and x_b. Thus one measures directly (analogously to (12.2.12))

$$A_{LL}^{\chi_2} = -\frac{\Delta G(x_a)}{G(x_a)} \frac{\Delta G(x_b)}{G(x_b)}. \tag{12.2.26}$$

If there is a significant contribution from reaction B in Fig. 12.7 the effective gluon polarization gets smeared out by an integration over, say, x_a, and the partonic asymmetry is no longer maximal. $a_{LL}^{GG \to \chi_2 G}$ is shown in Fig. 12.9 in the limit $\hat{t} \to 0$ as function of $M^2/\hat{s}$. The hadronic asymmetry will thus be smaller than predicted by (12.2.26) but should still yield measurable values. This depends, however, upon ensuring that the collision energy is not too large, i.e. not forcing x_a, x_b to be too small, since one expects $\Delta G(x)/G(x)$ to tend to zero as $x \to 0$.

There is also the problem that the theory is somewhat less reliable when more than one partonic channel contributes. Suppose there are two channels (A) and (B). From the intuitive expression (12.2.13) we will have

$$\begin{aligned} A_{LL} &= \left(\frac{\Delta\sigma_A}{\sigma_A + \sigma_B}\right) + \left(\frac{\Delta\sigma_B}{\sigma_A + \sigma_B}\right) \\ &= \left(\frac{\sigma_A}{\sigma_A + \sigma_B}\right) \hat{a}_{LL}^A + \left(\frac{\sigma_B}{\sigma_A + \sigma_B}\right) \hat{a}_{LL}^B \end{aligned} \tag{12.2.27}$$

https://doi.org/10.1017/9781009402040.012 Published online by Cambridge University Press

and various uncertain factors, such as K-factors, non-relativistic radial wave-function values etc., no longer cancel out in the asymmetry. In practice this may not be a serious problem but must be investigated.

J/Ψ production. If the χ_2 particles cannot be reconstructed adequately one can get less clean information from the J/Ψ asymmetry. All three processes A, B and C in Fig. 12.7 now contribute, since the branching ratio $BR(\chi_2 \to J/\Psi\gamma) \approx 14\%$ is sizeable. The same gluon polarization appears, but the partonic asymmetry is diluted since $\hat{a}_{LL}(GG \to J/\Psi G)$ is generally *positive*.

The integrated partonic cross-section asymmetry is shown versus $M^2/\hat{s}$ in Fig. 12.9. It would seem from this that the hadronic asymmetry ought to be reasonably sensitive to the structure of $\Delta G(x)$, but detailed calculations, using up-to-date parametrizations of $\Delta G(x)$, are needed.

12.2.5 Semi-inclusive lepton–hadron scattering

Consider the deep inelastic scattering of a charged lepton l, momentum k^μ, on a nucleon N, momentum P^μ:

$$l + N \to l + C + X, \tag{12.2.28}$$

where C is some identified hadron, set of hadrons or jet. We assume that lepton and proton are longitudinally polarized. The incoming lepton and the exchanged photon have energies E and ν respectively, in the Lab.

Of particular interest is the case of charm production since it is controlled by the mechanism in Fig. 11.11 and may prove to be one of the best ways to learn about the polarized gluon density. The cross-section for

$$l + p \to l + (c\bar{c}) + X, \tag{12.2.29}$$

based upon the mechanism depicted in Fig. 11.11, can be expressed in terms of various cross-sections $\hat{\sigma}, \hat{\sigma}_0, \Delta\hat{\sigma}$ for the partonic reaction

$$\text{`}\gamma\text{'} + G \to c + \bar{c}. \tag{12.2.30}$$

For real photons the flux factor needed in calculating a cross-section is $K = \nu$. For virtual photons there is no unambiguous definition. It is simply a matter of convention, provided only that $K = \nu$ at $Q^2 = 0$. Various conventions for K exist in the literature: $\sqrt{\nu^2 + Q^2}$, $\nu - Q^2/(2M)$, $\nu/\sqrt{1 + Q^2/\nu^2}$, but clearly the *physical* cross-section for any reaction is independent of the choice of K.

https://doi.org/10.1017/9781009402040.012 Published online by Cambridge University Press

For the reaction (12.2.29) one has

$$\frac{d\sigma^{\rightarrow}_{\Leftarrow}}{dvdQ^2} + \frac{d\sigma^{\rightarrow}_{\Rightarrow}}{dvdQ^2}$$
$$= \frac{\alpha K}{2\pi Q^2 v^2} \int_{x_{\min}}^{x_{\max}} dx G(x) \left\{ \left[1 + (1-y)^2\right] \hat{\sigma}(\hat{s}, Q^2) + 2(1-y)\hat{\sigma}_0(\hat{s}, q^2) \right\} \tag{12.2.31}$$

$$\frac{d\sigma^{\rightarrow}_{\Leftarrow}}{dvdQ^2} - \frac{d\sigma^{\rightarrow}_{\Rightarrow}}{dvdQ^2} = \frac{\alpha K}{2\pi Q^2 v^2} \left[1 - (1-y)^2\right] \int_{x_{\min}}^{x_{\max}} dx \Delta G(x) \Delta\hat{\sigma}(\hat{s}, Q^2) \tag{12.2.32}$$

where

$$y \equiv \frac{P \cdot q}{P \cdot k} = \frac{v}{E} \tag{12.2.33}$$

$$\hat{s} = (q + xP)^2 \approx 2Mvx - Q^2 \tag{12.2.34}$$

and the range of integration variable x corresponds to the requirement on the charm-quark mass

$$4m_c^2 \leq \hat{s} \leq s = 2Mv - Q^2. \tag{12.2.35}$$

Expressed in terms of cross-sections with fixed initial state helicities, the 'γ' $G \to c\bar{c}$ partonic cross-sections are

$$\begin{aligned} \hat{\sigma} &= \hat{\sigma}_{++} + \hat{\sigma}_{-+} \\ \Delta\hat{\sigma} &= \hat{\sigma}_{++} - \hat{\sigma}_{-+} \\ \hat{\sigma}_0 &= \hat{\sigma}_{0+} + \hat{\sigma}_{0-}. \end{aligned} \tag{12.2.36}$$

The results for the partonic cross-sections can be extracted from the calculations of Jones and Wyld (1978), Watson (1982) and Glück and Reya (1988). One finds

$$\hat{\sigma}(\hat{s}, Q^2) = \frac{2\pi\alpha_s \alpha e_c^2}{\hat{s}\left[1 + (Q^2/\hat{s})\right]^3} \left(\frac{v}{K}\right) \left\{ -\beta(2-\beta^2) + \frac{1}{2}(3-\beta^4) \ln\left(\frac{1+\beta}{1-\beta}\right) + 2\frac{Q^2}{\hat{s}}\beta + \frac{Q^4}{\hat{s}^2}\left[\ln\left(\frac{1+\beta}{1-\beta}\right) - \beta\right] \right\} \tag{12.2.37}$$

$$\Delta\hat{\sigma}(\hat{s}, Q^2) = \frac{2\pi\alpha_s \alpha e_c^2}{\hat{s}\left[1 + (Q^2/\hat{s})\right]^3} \left(\frac{v}{K}\right) \left\{ \ln\left(\frac{1+\beta}{1-\beta}\right) - 3\beta - 2\frac{Q^2}{\hat{s}}\beta + \frac{Q^4}{\hat{s}^2}\left[\beta - \ln\left(\frac{1+\beta}{1-\beta}\right)\right] \right\} \tag{12.2.38}$$

https://doi.org/10.1017/9781009402040.012 Published online by Cambridge University Press

$$\hat{\sigma}_0(\hat{s}, Q^2) = \frac{2\pi\alpha_s \alpha e_c^2}{\hat{s}\left[1 + (Q^2/\hat{s})\right]^3} \left(\frac{v}{K}\right) \frac{Q^2}{\hat{s}} \left\{2\beta + (\beta^2 - 1) \ln\left(\frac{1+\beta}{1-\beta}\right)\right\} \tag{12.2.39}$$

where

$$\beta = \sqrt{1 - 4m_c^2/\hat{s}} \tag{12.2.40}$$

and $e_c^2 = 4/9$.

In the above we have not shown the scale μ^2 at which $G(x)$ and $\Delta G(x)$ are to be evaluated. It should be clear from Fig. 11.11 that the scale is not Q^2, and it can be argued that the relevant scale is $\mu^2 \approx \hat{s}$.

In practice, because the cross-sections (12.2.31), (12.2.32) drop rapidly with Q^2, the first planned experiments will concentrate on small Q^2, where it is probably safe to put $Q^2 = 0$ in the expressions (12.2.37)–(12.2.39) for the partonic cross-sections. However, this is only justified if $Q^2/\hat{s}$ is negligible, and since $\hat{s}$ can be as small as $4m_c^2$ the approximation really requires $Q^2 \ll 4m_c^2$.

The partonic longitudinal asymmetry

$$\hat{a}_{LL}^{c\bar{c}} \equiv \frac{\Delta\hat{\sigma}(\hat{s}, q^2)}{\hat{\sigma}(\hat{s}, q^2)} \tag{12.2.41}$$

has an interesting shape as a function of β. At threshold, $\beta = 0$ and $\hat{a}_{LL}^{c\bar{c}} = -1$, whereas at infinite energy, $\beta \to 1$ and $\hat{a}_{LL}^{c\bar{c}} \to 1$ and this is true for all Q^2.

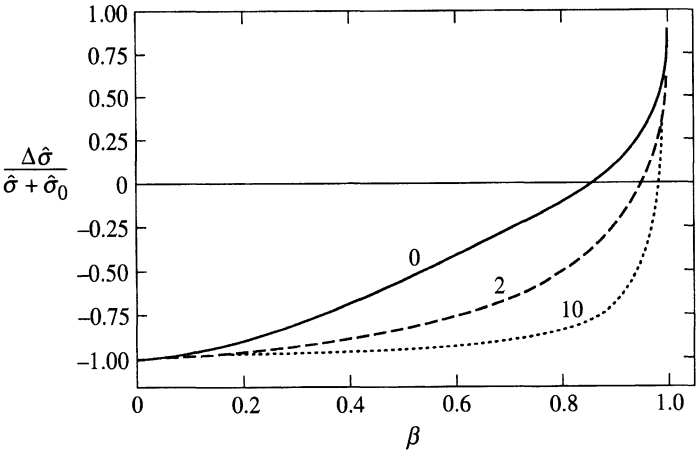

Fig. 12.10 The asymmetry $\Delta\hat{\sigma}/(\hat{\sigma} + \hat{\sigma}_0)$, which is effectively equal to $\hat{a}_{LL}^{c\bar{c}}$, as a function of β for three values of $Q^2/4m_c^2$.

https://doi.org/10.1017/9781009402040.012 Published online by Cambridge University Press

In Fig. 12.10 we show $\Delta\hat{\sigma}/(\hat{\sigma}+\hat{\sigma}_0)$ as a function of β for three values of $Q^2/4m_c^2$. In fact the rôle of $\hat{\sigma}_0$ is completely negligible, for two reasons: firstly $\hat{\sigma}_0/\hat{\sigma}$ is generally very small and secondly $\hat{\sigma}_0/\hat{\sigma}$ reaches its maximum of 10%–20% just where $\Delta\hat{\sigma}\approx 0$.

The $ep\to e+(c\bar{c})+X$ cross-sections (12.2.31) and (12.2.32) involve an integration over x or, equivalently, over $\hat{s}$ or β (see (12.2.34) and (12.2.40)); there will thus be a diminution of the cross-section difference (12.2.32), and therefore of the asymmetry, owing to a cancellation between the regions where $\hat{a}_{LL}^{c\bar{c}}$ is negative and those where it is positive, if $\Delta G(x)$ is monotonic. This effect grows in importance as v increases, since larger v implies larger $\beta_{\max}$ in the integration.

The effect of the cancellation can be combatted by going to larger Q^2, as can be seen from Fig. 12.10, but, as mentioned, one loses event rate.

In the approximation $Q^2=0$ one has for the measured asymmetry, upon changing integration variable from x to $\hat{s}$,[1]

$$A_{\parallel}^{c\bar{c}X}(E,v,Q^2=0)\equiv\left(\frac{d\sigma^{\vec{}}_{\Leftarrow}}{dv\,dQ^2}-\frac{d\sigma^{\vec{}}_{\Rightarrow}}{dv\,dQ^2}\right)\Big/\left(\frac{d\sigma^{\vec{}}_{\Leftarrow}}{dv\,dQ^2}+\frac{d\sigma^{\vec{}}_{\Rightarrow}}{dv\,dQ^2}\right)$$
$$=\left[\frac{1-(1-y)^2}{1+(1-y)^2}\right]\frac{\int_{4m_c^2}^{2Mv}d\hat{s}\,\Delta G(x=\hat{s}/(2Mv),\hat{s})\,\Delta\hat{\sigma}^{\gamma G}(\hat{s},Q^2=0)}{\int_{4m_c^2}^{2Mv}d\hat{s}\,G(x=\hat{s}/(2Mv),\hat{s})\,\hat{\sigma}^{\gamma G}(\hat{s},Q^2=0)}. \tag{12.2.42}$$

It is unfortunate that in (12.2.42) the parton densities are in principle integrated over both the gluon momentum fraction x and the hard scale $\hat{s}$. It would be much simpler, from a theoretical point of view, if one could measure cross-sections differential in $\hat{s}$.

An idea of the size of the asymmetry at $E=100$ GeV and $Q^2=0$, and its sensitivity to various models for $\Delta G(x)$, due to Gehrmann and Stirling (1996), is shown in Fig. 12.11. The sign, and the rapid change with energy for model C, is a consequence of the change in sign of $\Delta G(x)$ at $x\approx 0.1$.

12.3 Parity-violating longitudinal single-spin asymmetries

In a parity-conserving theory, if only one of the initial hadrons is polarized one has

$$d\sigma_+ = d\sigma_- \tag{12.3.1}$$

i.e. there is no asymmetry under reversal of helicity. However, in electroweak reactions such as the production of $W^{\pm}$ and Z^0, and in the

[1] Here we use the designation $A_{\parallel}$ that is conventional in papers on this subject.

https://doi.org/10.1017/9781009402040.012 Published online by Cambridge University Press

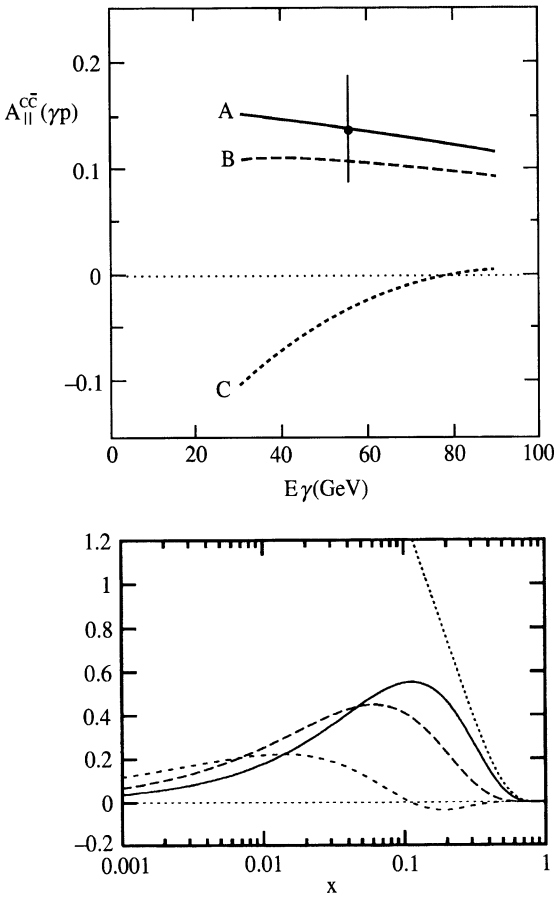

Fig. 12.11 The longitudinal asymmetry $A_{\parallel}^{c\bar{c}}$ vs. E_{γ}, for $lp \to l(c\bar{c})X$ at $E = 100$ GeV and $Q^2 = 0$. The data point with error bar indicates the expected accuracy in the COMPASS experiment at CERN; the curves correspond to $x\Delta G(x, 4\ \text{GeV}^2)$ in *NLO* for the three models of $\Delta G(x)$ shown in the lower figure (courtesy of G. Mallot and T. Gehrmann.) In the latter figure the dotted line gives $xG(x)$.

production of very massive Drell–Yan pairs where Z^0 exchange is important, parity is not conserved and one obtains interesting information from the longitudinal single-spin asymmetries.

12.3.1 *Small-p_T single-spin $W^{\pm}$ and Z^0 production*

The production of $W^{\pm}$ and Z^0 in Drell–Yan-type reactions at *small* p_T should provide a formidable test for our knowledge of the polarized *sea-quark* densities at the huge scale of $Q^2 \approx M_W^2$.

https://doi.org/10.1017/9781009402040.012 Published online by Cambridge University Press

Consider production of W^+ in

$$\vec{p}_A + p_B \to W^+ + X$$

with the axis OZ taken along the momentum of the longitudinally polarized proton, labelled A, which collides with the unpolarized target proton B.

The W^+ is produced with 4-momentum $p^\mu \approx (p^0, 0, 0, p_z)$ and rapidity

$$y = \frac{1}{2} \ln \left(\frac{p^0 + p_z}{p^0 - p_z} \right). \tag{12.3.2}$$

Since only left-handed u quarks and right-handed $\bar{d}$ antiquarks can couple to the W^+ one has

$$\begin{aligned} d\sigma_+ &\propto u_-(x_a)\bar{d}_+(x_b) + \bar{d}_+(x_a)u_-(x_b) \\ &\propto u_-(x_a)\bar{d}(x_b) + \bar{d}_+(x_a)u(x_b) \end{aligned} \tag{12.3.3}$$

since, with B unpolarized, for any parton $q_+(x) = q_-(x) = q(x)/2$.

Similarly

$$d\sigma_- \propto u_+(x_a)\bar{d}(x_b) + \bar{d}_-(x_a)u(x_b) \tag{12.3.4}$$

Thus the parity-violating longitudinal spin asymmetry is[1]

$$A_L^{W^+} = \frac{d\sigma_- - d\sigma_+}{d\sigma_- + d\sigma_+} = \frac{\Delta u(x_a)\bar{d}(x_b) - \Delta\bar{d}(x_a)u(x_b)}{u(x_a)\bar{d}(x_b) + \bar{d}(x_a)u(x_b)} \tag{12.3.5}$$

where

$$x_a = \sqrt{\tau}e^y \qquad x_b = \sqrt{\tau}e^{-y} \tag{12.3.6}$$

with, here,

$$\tau = M_W^2/s \tag{12.3.7}$$

and where the parton densities should be evaluated at a scale $Q^2 \approx M_W^2$.

For the production of W^- one has

$$A_L^{W^-} = \frac{\Delta d(x_a)\bar{u}(x_b) - \Delta\bar{u}(x_a)d(x_b)}{d(x_a)\bar{u}(x_b) + \bar{u}(x_a)d(x_b)}. \tag{12.3.8}$$

As pointed out by Bourrely and Soffer (1993), the expressions (12.3.5) and (12.3.8) take a particularly simple form in certain kinematic regimes.

For $y = 0$ one has $x_a = x_b = \sqrt{\tau}$ and

$$\begin{aligned} A_L^{W^+} &= \frac{1}{2}\left(\frac{\Delta u}{u} - \frac{\Delta\bar{d}}{\bar{d}}\right) \\ A_L^{W^-} &= \frac{1}{2}\left(\frac{\Delta d}{d} - \frac{\Delta\bar{u}}{\bar{u}}\right) \end{aligned} \tag{12.3.9}$$

[1] We here follow the sign convention of Bourrely and Soffer (1993).

https://doi.org/10.1017/9781009402040.012 Published online by Cambridge University Press

For large negative y, x_a is small and x_b large so that, for the antiquark, $\bar{q}(x_b)$ should be negligible. Hence

$$A_L^{W^+} \approx -\frac{\Delta\bar{d}(x_a)}{\bar{d}(x_a)} \qquad A_L^{W^-} \approx -\frac{\Delta\bar{u}(x_a)}{\bar{u}(x_a)}. \tag{12.3.10}$$

Similarly, for y large and positive, x_a is large, so

$$A_L^{W^+} \approx \frac{\Delta u(x_a)}{u(x_a)} \qquad A_L^{W^-} \approx \frac{\Delta d(x_a)}{d(x_a)}. \tag{12.3.11}$$

For the productions of Z^0 at *small* p_T, the argument leading to (12.3.5) is slightly complicated by the fact that both left- and right-handed quarks can couple to Z^0 with a strength that can be read off from (9.1.8). One ends up with

$$A_L^{Z^0} = \frac{\sum_f \mathscr{A}_f \left[\Delta\bar{q}_f(x_a)q_f(x_b) - \Delta q_f(x_a)\bar{q}_f(x_b)\right]}{\sum_f \left[\bar{q}_f(x_a)q_f(x_b) + q_f(x_a)\bar{q}_f(x_b)\right]} \tag{12.3.12}$$

where $f = u, d$ and $\mathscr{A}_f$ is defined in (9.2.13) and (9.1.5).

Some estimates of the single-spin parity-violating asymmetries, as a function of y, at $\sqrt{s} = 500$ GeV, for $W^\pm$ and Z^0 with very small transverse momentum, are shown in Figs. 12.12 and 12.13. The solid curves correspond to a reasonable choice of sea-quark polarization; the broken curves have $\Delta\bar{u} = \Delta\bar{d} = 0$. It is seen that there are regions for W^- and Z^0 production where there is significant sensitivity to the sea-quark polarization. This is not so for W^+ production, since it is dominated by the large positive up-quark polarization.

12.3.2 *Larger-p_T single-spin $W^\pm$ production*

We consider the production of $W^\pm$ with 4-momentum $q^\mu = (q_0, \mathbf{q}_T, q_z)$, where q_T need not be small, in collisions of a proton (A) with longitudinal polarization $\mathscr{P}$, and an unpolarized proton or antiproton (B):

$$\vec{p}_A(\mathscr{P}) + (p_B \text{ or } \bar{p}_B) \to W^\pm + X. \tag{12.3.13}$$

The Z-axis lies along the momentum of the polarized proton. Several partonic processes contribute to the reaction: (a) Drell–Yan $q\bar{q} \to W$, (b) $q\bar{q} \to WG$ and (c) $qG \to Wq$. However, there are two kinematic regions where (a) and (b) dominate and where, consequently, the results depend principally on the quark and antiquark distributions. They are specified as region 1,

$$q_z > 0 \qquad q_z \gtrsim 2q_T \qquad q_T \ll M_W,$$

https://doi.org/10.1017/9781009402040.012 Published online by Cambridge University Press

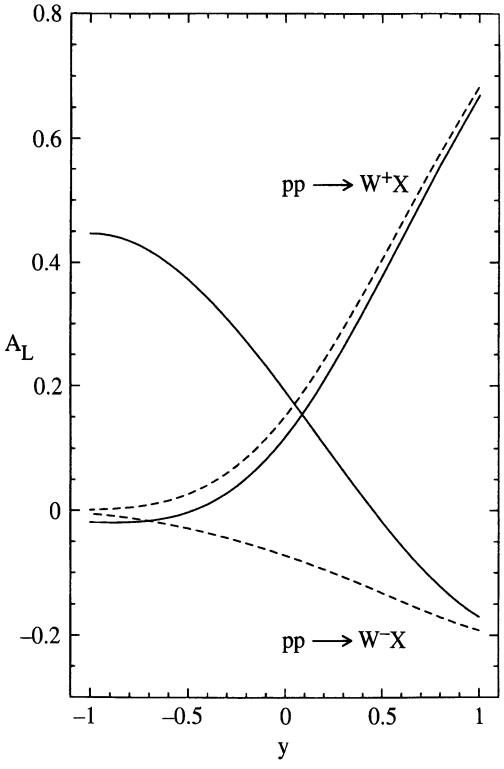

Fig. 12.12 Single-spin parity-violating asymmetry in $\vec{p}p \to W^{\pm}X$ vs. rapidity y at $\sqrt{s} = 500$ GeV for $W^{\pm}$with very small transverse momentum (from Bourrely and Soffer, 1993). For an explanation of the curves see the text.

and region 2,

$$q_z < 0 \qquad |q_z| \gtrsim 2q_T \qquad q_T \leq \bar{q}(s),$$

where $\bar{q}(s)$ is plotted in Fig. 12.14. The results that follow (Leader, 1986) are reliable only in regions 1 and 2.

In these regions the momentum fractions carried by the partons can be approximated by

$$\begin{aligned} x_a \equiv \hat{x}_a &= \frac{1}{\sqrt{s}}(q_0 + q_z + q_T) \\ x_b \equiv \hat{x}_b &= \frac{1}{\sqrt{s}}(q_0 - q_z + q_T) \end{aligned} \tag{12.3.14}$$

with $q^2 \approx M_W^2$, provided that $\hat{x}_{a,b} \ll 1$.

In the specified kinematic regions the normalized decay angular distribution for the $l^{\pm}$, in the rest frame of the $W^{\pm}$, with OZ along the motion

https://doi.org/10.1017/9781009402040.012 Published online by Cambridge University Press

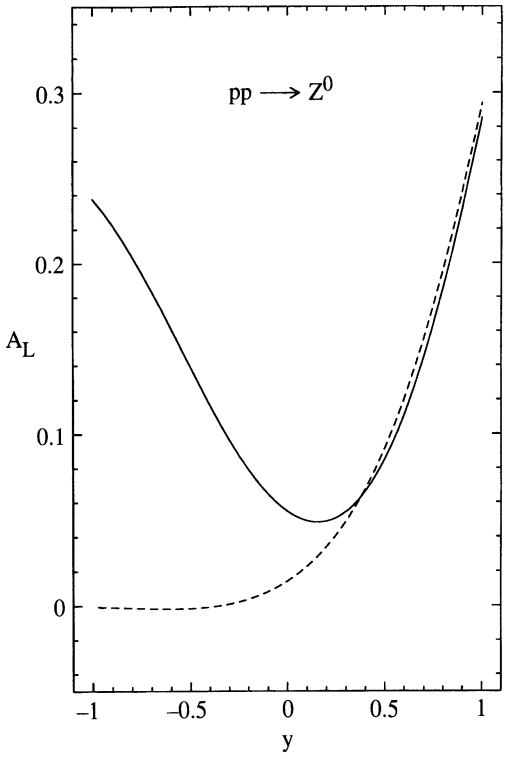

Fig. 12.13 Single-spin parity-violating asymmetry in $\vec{p}p \to Z^0X$ vs. rapidity y at $\sqrt{s} = 500$ GeV for Z^0 with small transverse momentum (from Bourrely and Soffer, 1993). For curves see the text.

of the $W^{\pm}$, may be taken to be[1]

$$W_{\pm}(\theta_l, \phi_l) \approx \frac{3}{16}\left(1 + \cos^2\theta_l \pm 2\mathscr{P}_{\pm}\cos\theta_l\right) \tag{12.3.15}$$

where $\mathscr{P}_{\pm}$ is the helicity polarization of the produced $W^{\pm}$. Experimental study of the decay distribution yields the values of $\mathscr{P}_{\pm}$.

The results are most simply expressed in term of the auxiliary quantities

$$\begin{aligned} \alpha_{\pm}(q_z, q_T; \mathscr{P}) &\equiv \frac{1+\mathscr{P}_{\pm}}{1-\mathscr{P}_{\pm}} \qquad \text{for } q_z > 0 \\ &\equiv \frac{1-\mathscr{P}_{\pm}}{1+\mathscr{P}_{\pm}} \qquad \text{for } q_z < 0 \end{aligned} \tag{12.3.16}$$

[1] We have used eqns (3.1.70) and (8.2.20) and the fact that in the above kinematic regions the Ws are produced predominantly with helicity ± 1.

https://doi.org/10.1017/9781009402040.012 Published online by Cambridge University Press

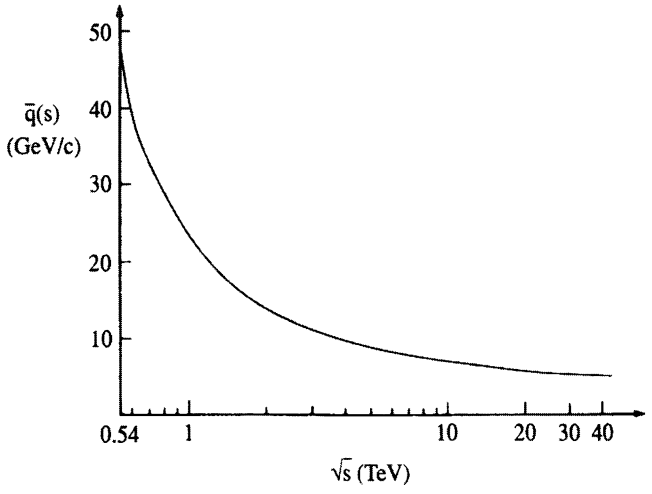

Fig. 12.14. The function $\bar{q}(s)$ vs. $\sqrt{s}$.

and in the comparison of these quantities for polarized and unpolarized protons, i.e. by constructing the ratio

$$r_{\pm}(q_z, q_T; \mathscr{P}) \equiv \frac{\alpha_{\pm}(q_z, q_T; \mathscr{P})}{\alpha_{\pm}(q_z, q_T; 0)}. \tag{12.3.17}$$

Then, for the various reactions one has

$$\text{for} \quad \left.\begin{array}{l} \vec{p} + p \to W^+ + X \\ \vec{p} + \bar{p} \to W^+ + X \end{array}\right\} \quad r_+(q_z, q_T; \mathscr{P}) = \frac{1 + \mathscr{P}\Delta\bar{d}(\hat{x}_a)/\bar{d}(\hat{x}_a)}{1 - \mathscr{P}\Delta u(\hat{x}_a)/u(\hat{x}_a)} \tag{12.3.18}$$

$$\text{for} \quad \left.\begin{array}{l} \vec{p} + p \to W^- + X \\ \vec{p} + \bar{p} \to W^- + X \end{array}\right\} \quad r_-(q_z, q_T; \mathscr{P}) = \frac{1 + \mathscr{P}\Delta\bar{u}(\hat{x}_a)/\bar{u}(\hat{x}_a)}{1 - \mathscr{P}\Delta d(\hat{x}_a)/d(\hat{x}_a)} \tag{12.3.19}$$

where the parton densities are at scale $q^2 = M_W^2$.

It should be noted that, whereas the $r_{\pm}$ are the same for proton–proton and proton–antiproton collisions, the $\alpha_{\pm}$ are quite different (see Leader, 1986) and it may turn out that the $\alpha_{\pm}$ for $p\bar{p}$ collisions are too small for a significant measurement in practice — indeed, early tests of the standard model assumed $\alpha_{\pm} = 0$ for the $p\bar{p}$ collisions at the CERN collider.

Note that if one can observe the process

$$\vec{p}_A + (p_B \text{ or } \bar{p}_B) \to W^{\pm}(\mathbf{q}) + \text{jet}(\mathbf{k}) \tag{12.3.20}$$

https://doi.org/10.1017/9781009402040.012 Published online by Cambridge University Press

then (12.3.14) can be replaced by the exact equations

$$x_a = \frac{1}{\sqrt{s}}(q_0 + k_0 + q_z + k_z)$$
$$x_b = \frac{1}{\sqrt{s}}(q_0 + k_0 - q_z - k_z). \tag{12.3.21}$$

Note also that the validity of the whole approach can be checked by testing whether the measured quantities in (12.3.18) and (12.3.19) are independent of x_b, as they are supposed to be.

Finally, it is a nice feature that the measurement of $r_\pm$ gives information directly about the *polarization* of the quarks and antiquarks, i.e. about $\Delta q(x)/q(x)$, a quantity that is of interest because of theoretical ideas about its behaviour for small and large x (see subsection 11.7.1).

12.3.3 Larger-p_T single-spin massive Drell-Yan production

For a Drell–Yan reaction where the lepton pair is produced with non-negligible transverse momentum, the analogue of (12.3.20) is

$$\frac{d^4\sigma_{+/-}}{dx_T dy d\tau d\cos\theta_l} = \sum_{j=0}^{2} D^j_{+/-} Y_{j0}(\theta_l) \tag{12.3.22}$$

and the single-spin longitudinal asymmetries are

$$A_L^j = \frac{D_+^j - D_-^j}{D_+^j + D_-^j}. \tag{12.3.23}$$

Because parity violation only becomes significant when Z^0 exchange starts to be important, one finds that the A_L^j are exceedingly small for $M \ll M_Z$. However, as seen in Fig. 12.15 the asymmetry is fairly large for $M = M_Z$ and discriminates quite well between the polarized gluon densities described in (12.2.22).

12.4 Transverse two-spin asymmetries

We consider a transversely polarized beam and target in a parity conserving theory. Particle A is taken to be incoming along OZ and we fix the X-axis to lie along the polarization of particle A. The spin directions of A and B are denoted by $\uparrow\uparrow$ or $\uparrow\downarrow$, corresponding to the transverse covariant spin vector of B being either along or opposite to that of A. The final state jet or hadron C emerges with azimuthal angle ϕ in the Lab.

https://doi.org/10.1017/9781009402040.012 Published online by Cambridge University Press

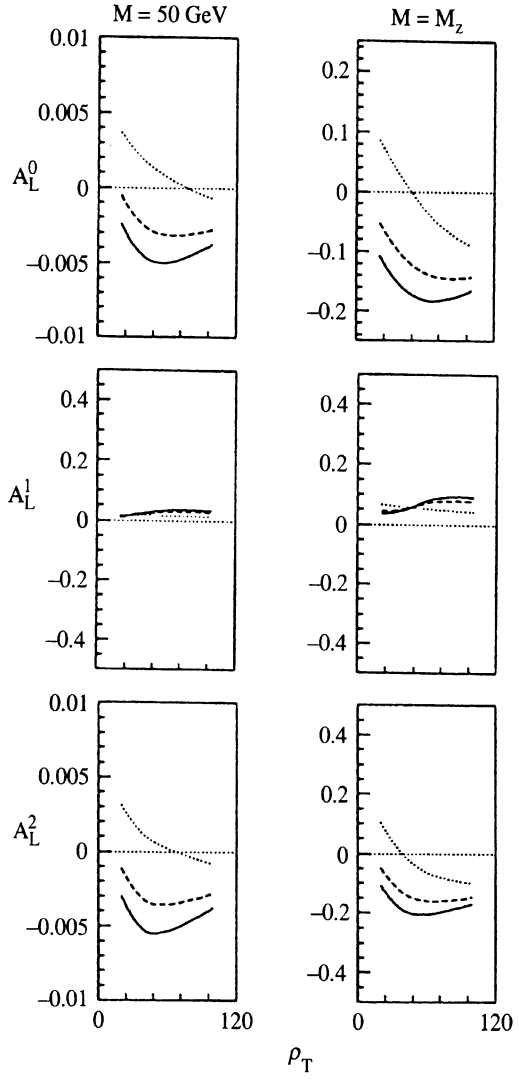

Fig. 12.15 The single-spin parity-violating Drell–Yan longitudinal asymmetries A_L^j vs. p_T for two values of M at $y = 0$. For the curves see the caption to Fig. 12.6. From Leader and Sridhar (1994), where A_L^j is labelled A_s^j ('s' for single).

Because the difference of cross-sections now depends upon ϕ, the expression (12.2.2) is somewhat altered. One defines

$$\frac{d^3\Delta_T\sigma}{d^3\mathbf{p}_C} \equiv \frac{d^3\sigma^{\uparrow\uparrow}}{d^3\mathbf{p}_C} - \frac{d^3\sigma^{\uparrow\downarrow}}{d^3\mathbf{p}_C} \tag{12.4.1}$$

https://doi.org/10.1017/9781009402040.012 Published online by Cambridge University Press

and finds

$$E_C \frac{d^3\Delta_T\sigma}{d^3\mathbf{p}_C} = 2\sum_{a,b,c,d}\int_{\xi_a} dx_a \int_{\xi_b} dx_b \Delta_T f_a^A(x_a)\Delta_T f_b^B(x_b) \times \frac{d^2\Delta_T\hat{\sigma}^{ab\to cd}}{d\hat{t}d\phi}(\hat{s},\hat{t},\phi)\frac{1}{z}D_C^c(z) \tag{12.4.2}$$

where

$$\frac{d^2\Delta_T\hat{\sigma}^{ab\to cd}}{d\hat{t}d\phi} \equiv \frac{d^2\hat{\sigma}^{\uparrow\uparrow}}{d\hat{t}d\phi} - \frac{d^2\hat{\sigma}^{\uparrow\downarrow}}{d\hat{t}d\phi}. \tag{12.4.3}$$

The transversely polarized parton densities $\Delta_T f$ that occur in (12.4.2) were introduced in Section 11.9; see eqn (11.9.15). Expressions for the integration limits and relations between x_a, x_b and $\hat{s}$ and $\hat{t}$ and definitions of other kinematic variables were given in Section 12.1. Because the partonic single spin asymmetries are zero in leading order, it follows from (5.6.12) that one can write

$$\frac{d^2\hat{\sigma}^{\uparrow\uparrow/\uparrow\downarrow}}{d\hat{t}d\phi} = \frac{1}{2\pi}\frac{d\hat{\sigma}}{d\hat{t}}\left[1 \pm \hat{a}_{TT}(\hat{s},\hat{t})\cos 2\phi\right] \tag{12.4.4}$$

so that

$$\frac{d^2\Delta_T\hat{\sigma}^{ab\to cd}}{d\hat{t}d\phi} = \frac{1}{\pi}\frac{d\hat{\sigma}}{d\hat{t}}\hat{a}_{TT}\cos 2\phi. \tag{12.4.5}$$

The double-spin partonic transverse asymmetry parameters $\hat{a}_{TT}$ are given in Table 12.3 for various reactions and shown as a function of the CM scattering angle θ^* in Fig. 12.16. Some of these results are due to Ranft and Ranft (1978), to Hidaka, Monsay and Sivers (1979) and to

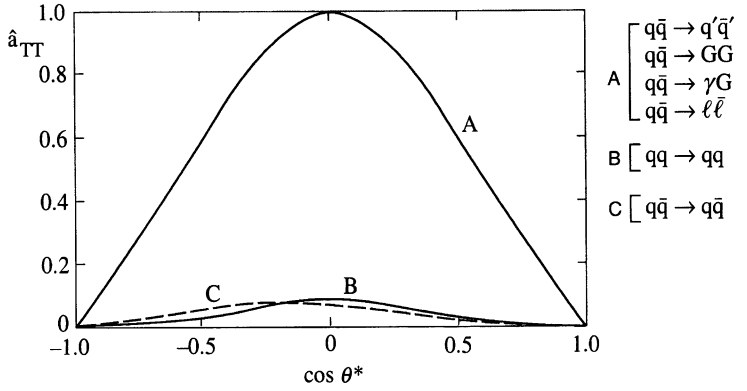

Fig. 12.16 Double-spin partonic transverse polarization asymmetry parameter vs. $\cos\theta^*$ for various partonic processes, in lowest order.

https://doi.org/10.1017/9781009402040.012 Published online by Cambridge University Press

Table 12.3. Partonic transverse double spin asymmetry parameter. A prime on q means that q' has different flavour from q.

Reaction	$\hat{a}_{TT}$
$qq \to qq$	$\dfrac{2\hat{t}^2\hat{u}^2/3}{\hat{u}^2(\hat{s}^2+\hat{u}^2)+\hat{t}^2(\hat{s}^2+\hat{t}^2)-(2\hat{s}^2\hat{t}\hat{u}/3)}$
$q\bar{q} \to q\bar{q}$	$\dfrac{2\hat{u}\hat{t}^2(\hat{t}-\hat{s}/3)}{\hat{s}^2(\hat{s}^2+\hat{u}^2)+\hat{t}^2(\hat{u}^2+\hat{t}^2)-(2\hat{u}^2\hat{s}\hat{t}/3)}$
$qq' \to qq'$ $q\bar{q}' \to q\bar{q}'$	0
$q\bar{q} \to q'\bar{q}'$ $q\bar{q} \to GG$	$\dfrac{2\hat{u}\hat{t}}{\hat{t}^2+\hat{u}^2}$
$q\bar{q} \to \gamma G$	$\dfrac{2\hat{u}\hat{t}}{\hat{u}^2+\hat{t}^2}$
$q\bar{q} \to \gamma \to l\bar{l}$	$\dfrac{2\hat{u}\hat{t}}{\hat{t}^2+\hat{u}^2}$

Jaffe and Saito (1996).[1] Others were calculated in an interesting paper of Artru and Mekhfi (1990).

It is seen that large asymmetries occur for $q\bar{q} \to q'\bar{q}', GG, \gamma G$ and $l\bar{l}$, the rest being an order of magnitude smaller. However, it is not at all clear how big the asymmetries will be at the hadronic level, since we have little knowledge about the transversely polarized parton densities which have never been measured directly; see, however, Section 13.3.

Various models for the $\Delta_T q(x)$ have been constructed, but none of them is very convincing. As mentioned in subsection 11.9.1, the one reliable result we have to guide us is the Soffer bound (Soffer, 1995):

$$|\Delta_T q(x)| \leq \tfrac{1}{2}\,[q(x) + \Delta q(x)]\,. \tag{12.4.6}$$

Since for d quarks $\Delta d(x)$ is negative and fairly large whereas $\Delta u(x)$ is large and positive, we might expect to have

$$|\Delta_T d(x)| \ll |\Delta_T u(x)|, \tag{12.4.7}$$

but this does not strictly follow from (12.4.6). Interestingly, however, an attempt to estimate $\Delta_T u(x)$ and $\Delta_T d(x)$ using QCD sum rules (Ioffe and

[1] Note that there are errors in these three papers.

https://doi.org/10.1017/9781009402040.012 Published online by Cambridge University Press

Khodjamirian, 1995), while only reliable in the range $0.3 \lesssim x \lesssim 0.5$ does suggest a large $\Delta_T u(x)$, with $|\Delta_T u(x)| > |\Delta u(x)|$, and $|\Delta_T d(x)| \ll |\Delta_T u(x)|$.

On the basis of non-relativistic models it has sometimes been supposed that $\Delta_T q(x) = \Delta q(x)$, but it is clear that such an assumption may violate (12.4.6), especially if Δq is negative.

Given the magnitudes of the partonic $\hat{a}_{TT}$, the best way to study the $\Delta_T q(x)$ would be via the small-p_T Drell-Yan reaction $p\bar{p} \to l\bar{l} + X$, with both beams transversely polarized, but there is no prospect of such a measurement in the foreseeable future. In reactions initiated by proton–proton collisions the hadronic asymmetry will be diminished by those partonic reactions with large cross-sections but small $\hat{a}_{TT}$, or worse, gluon–gluon reactions that give no contribution to the asymmetry. Drell-Yan reactions *at small* p_T at least do not suffer from the latter problem, but in pp collisions the relevant parton densities that enter are of the form $\Delta_T q(x_a)\Delta_T \bar{q}(x_b)$, and it may well be that the transversely polarized antiquark densities are very small.

Drell–Yan reactions at large p_T have been studied by Vogelsang and Weber (1993) and, more recently, by Martin, Schäfer, Stratman and Vogelsang (1997). In the earlier work, $\Delta_T q_V = \Delta q_V$ was assumed for the valence densities and two models for the antiquark $\Delta_T \bar{q}$ were studied. One, labelled (a), is small and negative; the other, (b), large and negative. The double-spin transverse asymmetry

$$A_{TT} = \frac{d\sigma^{\uparrow\uparrow} - d\sigma^{\uparrow\downarrow}}{d\sigma^{\uparrow\uparrow} + d\sigma^{\uparrow\downarrow}} \tag{12.4.8}$$

was analysed for various choices of cross-section, for example differential in the mass of the lepton pair or in the p_T of the photon (i.e. of the lepton pair) etc. Typically, at $\sqrt{s} = 100$ GeV, $M^2 = 49$ (GeV/c^2)^2 and $\cos 2\phi = 1$, $A_{TT}(p_T)$ is very small for $p_T \gtrsim 2$ GeV/c, of the order of a few per cent. Of course, in this region the fundamental lowest-order process, which has a large asymmetry, does not contribute. Its contribution in the integrated cross-section, defined as $d^2\sigma/dMd\phi$, is considerable, and $A_{TT}(M)$ is much larger. In fact the integrated A_{TT} is roughly a scaling function of $\tau = M^2/s$, apart from scale breaking in the parton densities, and is shown in Fig. 12.17 as a function of τ. Also shown is the difference between the leading-order, $O(\alpha^2)$, and the next-to-leading-order $O(\alpha^2\alpha_s)$, results. The parton densities used were at scale $M^2 = 49$ (GeV/c^2)^2.

In the more recent study cited above an attempt is made to estimate the maximum possible A_{TT} by suitably saturating the Soffer bound, i.e. by taking

$$\Delta_T(x, Q_0^2) = \tfrac{1}{2}\left[q(x, Q_0^2) + \Delta q(x, Q_0^2)\right]. \tag{12.4.9}$$

https://doi.org/10.1017/9781009402040.012 Published online by Cambridge University Press

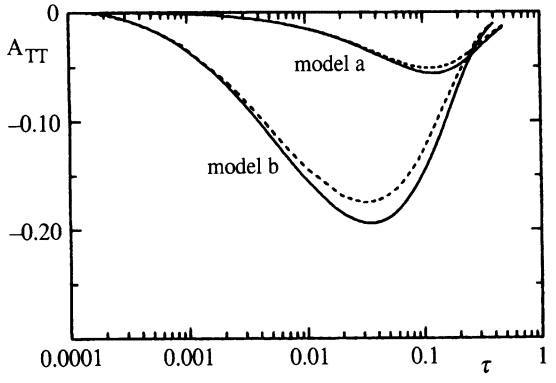

Fig. 12.17 The double-spin transverse asymmetry for the integrated Drell–Yan cross sections for $pp \to l\bar{l} + X$ vs. $\tau = M^2/s$, for two models of $\Delta_T \bar{q}(x)$; see text. Solid lines, $O(\alpha^2 \alpha_s)$ calculation; broken lines, $O(\alpha^2)$ calculation. (From Vogelsang, 1993.)

The tricky question is the choice of Q_0^2 at which (12.4.9) is imposed. Imposing it at a low value of Q_0 is acceptable, because the evolution to larger Q^2 continues to respect (12.4.6), as demonstrated by Bourrely, Soffer and Teryaev (1998), whereas imposing (12.4.9) at high Q_0^2 will lead to a violation of (12.4.6) at $Q^2 < Q_0^2$.

In fact a very low scale, $Q_0 = 0.6$ GeV/c, is chosen, corresponding to using the parton densities of the so-called 'radiative parton model' of Glück, Reya, Stratmann and Vogelsang (1996).

The results of this study are shown in Figs. 12.18 and 12.19, which show both the asymmetry A_{TT} as function of the lepton pair mass M and the cross-section difference

$$\frac{d\Delta_T \sigma}{dM} = \left(\int_{-\pi/4}^{\pi/4} d\phi + \int_{3\pi/4}^{5\pi/4} d\phi - \int_{\pi/4}^{3\pi/4} d\phi - \int_{5\pi/4}^{7\pi/4} d\phi \right) \frac{d^2 \Delta_T \sigma}{dM d\phi} \tag{12.4.10}$$

at two different values $\sqrt{s} = 150$ GeV and $\sqrt{s} = 500$ GeV, corresponding to the lower and upper regions of the RHIC energy range. At the higher energy, where much larger massses M can be produced, both photon and Z^0 exchange have been included, and this leads to an interesting M-dependence of A_{TT}.

It is seen that the cross-section differences are small and that A_{TT}, which, it should not be forgotten, has been maximized, is at the level of 1%–4%. The 'error bars' shown are an estimate of the expected statistical errors assuming 70% beam polarization and integrated luminosities of 240 pb^{-1} and 800 pb^{-1} at $\sqrt{s} = 150$ GeV and $\sqrt{s} = 500$ GeV respectively.

https://doi.org/10.1017/9781009402040.012 Published online by Cambridge University Press

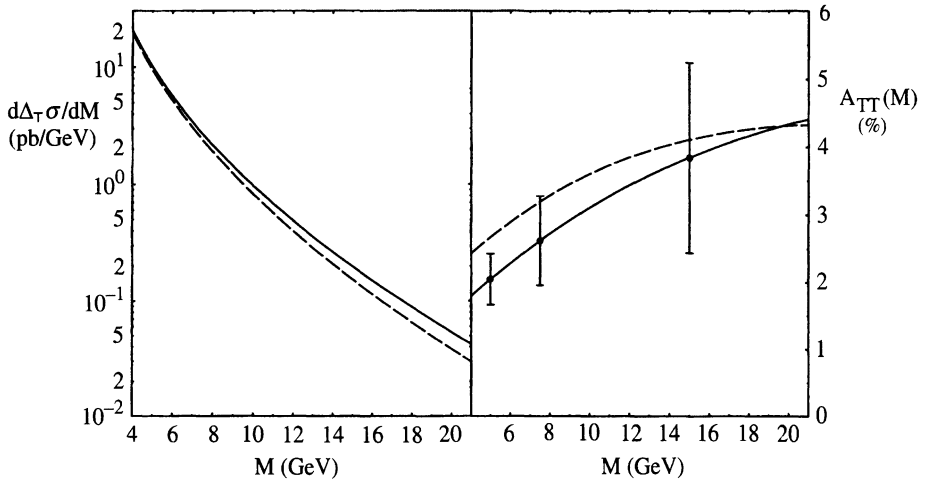

Fig. 12.18 $d\Delta_T\sigma/dM$ and A_{TT} vs. M for $\sqrt{s} = 150$ GeV. The solid lines are NLO, the broken line LO; see text. (Adapted from Martin, Schäfer, Stratman and Vogelsang, 1997.)

Of course, the asymmetries chosen by Nature could be considerably smaller than shown. It is thus not going to be easy to learn about the transverse densities $\Delta_T q(x)$, but with luck our first information should soon emerge from the RHIC programme. Another interesting source of information on $\Delta_T q(x)$ is discussed in Section 13.3.

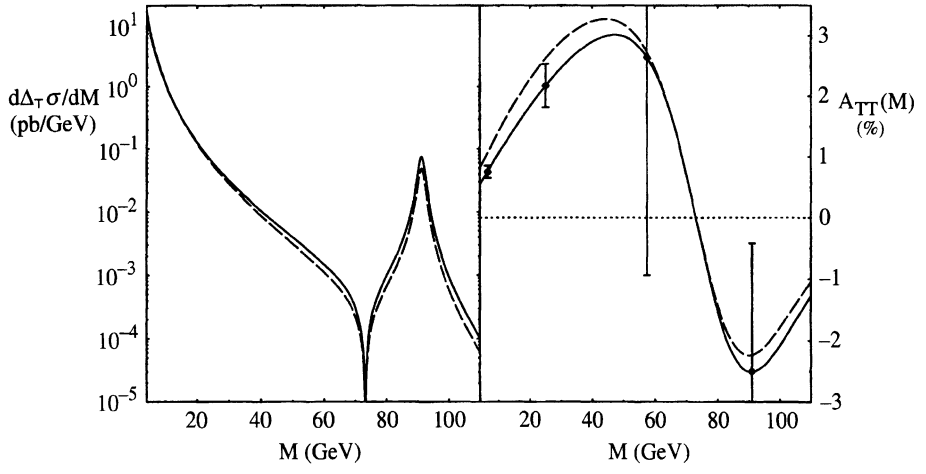

Fig. 12.19. As for Fig. 12.18 but at $\sqrt{s} = 500$ GeV

https://doi.org/10.1017/9781009402040.012 Published online by Cambridge University Press